Sensors and Process-Performance Interactions for Additive In-Mold Electronics in Automotive Applications

Pradeep Lall, Ved Soni, Fatahi Musa, Md Golam Sarwar
Auburn University
Electronics Packaging Research Institute
AL, USA
lall@auburn.edu

Scott Miller
NextFlex National Manufacturing Institute
CA, USA

ABSTRACT
The development of additively manufactured electronics processes has made it possible to integrate safety features into automotive touch surfaces for assessing driver alertness and stress levels. While current touch surfaces in vehicles are primarily for aesthetic purposes, the potential advancement through the integration of the human-machine interfaces using additively printed in-mold electronics presents interesting possibilities. However, the processes for printing sensors and integrating surface mount electronics for signal processing in additively printed conformal electronics are still not well understood. In-mold electronics offer opportunities for eliminating wire harnesses and reducing the vehicle's weight to meet stricter CO_2 emission standards and minimize the carbon footprint. This study investigates direct ink write and gravure offset print processes for thermo-formed in-mold electronics on various substrates. It also explores surface mount component attachment using conductive adhesive and the creation of signal processing and electrodermal sensors for measuring galvanic skin response, which is useful for assessing driver emotions and health. The objective of this study is to establish fabrication guidelines for in-mold electronic circuits, including ink print parameters, curing times for ink and adhesive, and thermoforming parameters to achieve optimal electrical performance and mold conformity.

Key words: Additive printed electronics, In-Mold electronics, Vacuum thermoforming, Stretchable ink, Gravure offset, Direct ink write

INTRODUCTION

The integration of advanced driver assistance systems (ADAS) in cars has introduced safety features like lane departure warning, driver alertness monitoring, collision avoidance, and cross-traffic alert. Currently, touch surfaces in vehicles serve mainly aesthetic purposes. A typical automobile may have as many as 50-70 control units that collect data from sensors and systems for autonomous decision-making, guidance, navigation, and control. The proliferation of ADAS has led to extensive use of wire harnesses and connectors in cars [1], [2], [8], with some wire harnesses weighing up to 36 kg [3], [4], posing challenges due to stricter CO_2 emission standards [5]. To address this, there's a push for lighter interconnection methods to reduce the carbon footprint [6]. Additively printed in-mold electronics (IMEs) offer a solution by integrating human-machine interfaces on touch surfaces and transmission of signals on thermoformed surfaces, allowing for the elimination of wire harnesses. The in-mold process involves depositing, curing, and forming conductive ink on thermoformable substrates, followed by low-pressure molding with thermoplastic polymer for encapsulation [7]. Material selection is critical for IME performance, process efficiency, and reliability, with specific inks designed to withstand thermoforming, enhance substrate adhesion, and suit processing conditions [8].

This study investigates the thermoforming process for printed conductive traces on polycarbonate (PC), High Impact Polystyrene (HIPS) and Polyethylene Glycol Terephthalate (PETG) substrates. The conductible ink printing has been achieved via gravure offset, direct write printing method and the samples have been thermoformed using a vacuum thermoforming system. Based on the recommended sintering conditions of the ink and the processing temperatures of both the substrates, different sintering and thermoforming parameters have been varied to determine the best-suited process recipe for minimizing the post-thermoforming line resistance and maximizing the adherence of the thermoformed substrate to the mold design. Finally, the feasibility of component-attached thermoformed samples alongside the realization of the functional circuits has also been investigated.

PROPERTIES AND TEST VEHICLE DESIGN

Conductive Materials and Substrate Properties

A silver conductive paste specifically designed for thermoforming has been used to print conductive traces for this study (properties listed in Table I) on both the direct ink write and gravure offset printing platforms. In addition, the properties of silver-based electrically conductive adhesive (ECA) ‘B’ used for component attachment are also included in Table I.Three thermoformable substrates have been used for this investigation: polycarbonate (PC), polyethylene glycol terephthalate (PETG), and high impact polystyrene (HIPS) whose properties have been mentioned in Table II.

Table I. Formable Conductive Ink 'A' & ECA 'B' Properties

Physical property	Ink 'A'	ECA 'B'
Conductive material	Silver	Silver
Solids % at 150 °C	64 – 70%	75 – 77%
Viscosity (cP)	10 – 18 kcP	40 – 90 kcP
Sheet Resistance (mΩ/sq/mil)	< 40	100 – 150
Recommended curing condition	20 min. at 120 °C	

Table II. Formable Substrate Properties

Property	PETG	PC	HIPS
Color	Clear	Clear	White, Black
Thickness	0.5 mm	0.25 mm, 0.5 mm	1.5mm
Heat Deflection Temperature	70 °C	153 °C	80 °C
VICAT Softening Temperature	83 °C	160 °C	90 °C

The thermoforming process relies on two key substrate properties: heat deflection temperature (HDT) and Vicat softening temperature (VST). HDT signifies the temperature at which the substrate bends under a specific load [9], while VST marks the temperature where it loses stiffness under penetration [10]. VST is generally always higher than HDT as the penetration load is generally higher than the bending load [11]. In the context of this study, the HDT has been defined as the limit at which the printed sample can be sintered to avoid substrate warpage, and VST is defined as the thermoforming temperature. Table 2 shows that PC has a higher HDT and VST than PETG and HIPS. In addition, as the recommended sintering condition for the ink is 20 minutes at 120°C, samples printed on PETG and HIPS must be sintered at a lower temperature for a longer time, and those printed on PC can be sintered at a higher temperature for a shorter time.

Test Vehicle Design

Direct Write

The direct write print platform for this study is nScrypt, a system capable of high precision in material deposition, making it suitable for applications that demand high accuracy, such as electronic printing or biomedical applications. The system has four printing heads, which include two smart pumps and two nFD pumps; the printing for this work has been conducted using the smart pumps (see Fig. 1). For the thermoforming study, printed samples were formed using a Formech 508FS vacuum-forming machine and a thermoforming mold (Fig. 2 (a)). The mold used for vacuum forming of samples for the trace reliability study is as shown in Fig. 2 (b), which includes features designed based on common surfaces present in automobiles: a cup holder, a volume knob, a switch (features A, B, and C respectively), and features D and E for resistance versus elongation studies. The study conducted on the direct write platform focuses on the labeled features A, B, and D. Two test vehicles used for this study are - Test Vehicle 01, intended for studying print process parameters and curing profiles, and Test Vehicle 02, designed to study thermoforming effect (see Fig. 3). Table III and Table IV presents the test matrix for print process study and sintering study respectively. Table V shows the test matrix employed for the thermoforming study for HIPS substrate.

(a) (b)

Fig. 1. (a) nScrypt direct write printer with its (b) Tool Heads

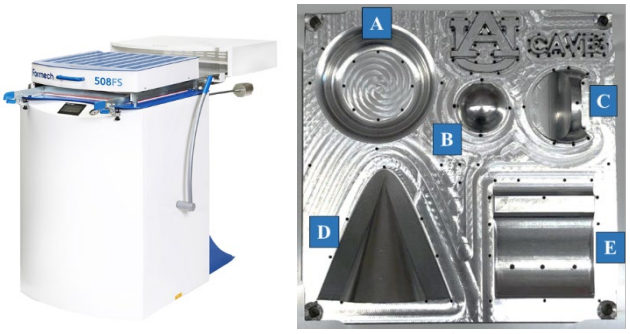

(a) (b)

Fig. 2. (a) Formech 508FS machine and (b) mold for Vacuum forming

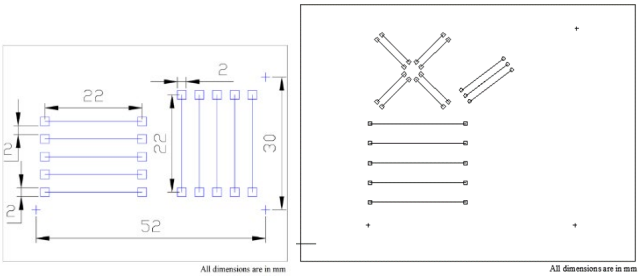

(a) (b)

Fig. 3. (a) Test Vehicle 01, (b) Test Vehicle 02

Table III. Printing Test Matrix

Parameters	Variation
Print Pressure	9 psi, 14 psi, 20 psi
Print Speed	1 mm/s, 3 mm/s, 5 mm/s
Stand-off Height	70 µm, 60 µm, 50 µm

Table IV. Sintering Test Matrix

Parameters	Variation
Temperature	70°C, 75°C, 80°C
Time (minutes)	60, 80, 100

Table V. Thermoforming study for HIPS substrate

Substrate	Forming Temperature	Forming Time
HIPS (ink curing: 60min. at 75°C)	150°C	25s, 30s, 35s
	175°C	25s, 30s, 35s
	200 °C	25s, 30s, 35s

Gravure Offset

The process of Gravure offset printing uses a single roller with a blanket to transfer patterns from the image plate to the substrate [12][13]. Fig. 4 (a) displays the schematic of the gravure offset image plate with 300 µm wide lines used for the trace thermoforming study along with the mold shown in Fig. 2 (b). Fig. 4 (b) shows the alignment of trace patterns on the image plate with the mold, highlighting variable features (A and D) experiencing different elongations due to their distinct topologies. The two quantities used for the quantification of the thermoforming process are resistance ratio (ratio of the post- to the pre-thermoforming R/L) and stretch ratio (ratio of the line lengths post- and pre-thermoforming) shown in equations (1) and (2) respectively.

$$\text{Resistance Ratio} = \frac{\text{Post-thermoforming R/L}}{\text{Pre-thermoforming R/L}} \quad (1)$$

$$\text{Stretch Ratio} = \frac{\text{Post-thermoforming Trace Length}}{\text{Pre-thermoforming Trace Length}} \quad (2)$$

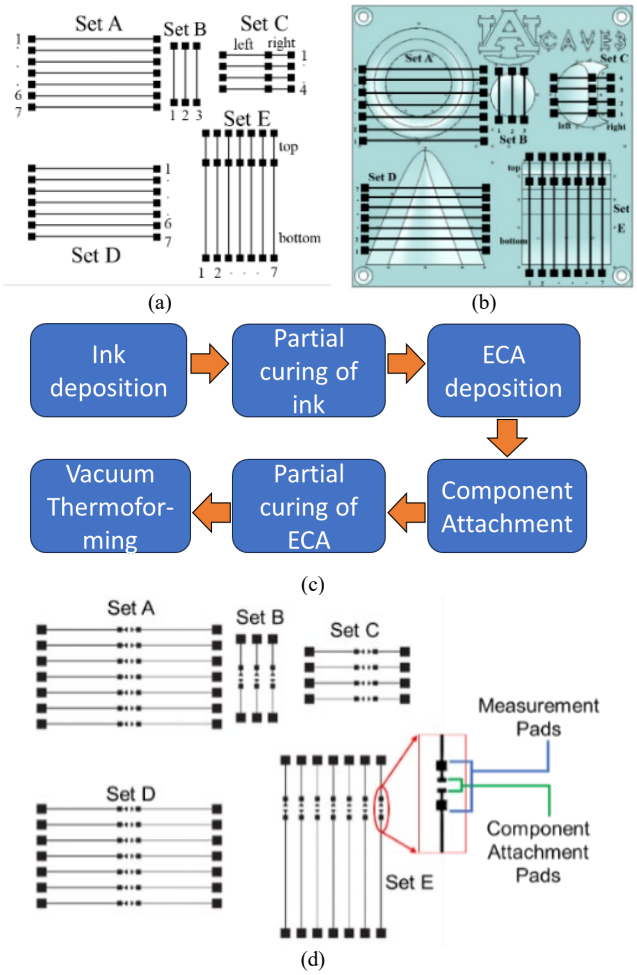

Fig. 4. (a) Gravure offset plate, (b) trace design overlapped with the mold (c) component attachment process flowchart, (d) plate for component attachment study

Since the aim of this study is to develop functional circuits on thermoformable substrates, a component attachment study was conducted using an 0805 size 42Ω SMD resistor for attachment via ECA 'B'. The process flow followed for producing component-attached conductible lines on thermoformed substrates is shown in Fig. 4 (c). The line design shown in Fig. 4 (a) was modified to include the measurement and component attachment pads (see Fig. 4 (d)) and the mold shown in Fig. 2 (b) was used for vacuum thermoforming. From the insights obtained from the initial studies, the ink and ECA curing temperatures were manipulated to minimize the curing time and to allow full sintering of the conductible materials on the formed sample. The resistance of the attached component was measured pre- and post-thermoforming using the measurement pads to select the best curing profile for the ECA. Table VI describes the thermoforming study for PC, wherein the thermoforming temperature and time varied. Considering the learning gained from the PC study, a thermoforming study was also conducted on the PETG substrate, with only varying thermoforming times. Table VII and Table VIII specifies the test matrix for the component attachment studies on PETG and PC, respectively.

Table VI: PC and PETG Thermoforming Study with Traces

Substrate	Forming temperature	Forming time
PC (ink curing: 10 min. at 140 °C)	200 °C	20s, 25s, 30s
	225 °C	15s, 20s, 25s
	250 °C	10s, 15s, 20s
PETG (ink cure: 60 min. at 70 °C)	125 °C	25s, 28s, 31s, 34s

Table VII: 0.5 mm PETG Component Attachment Study Test Matrix

Curing Temperature	Curing Time
70 °C	1 hr, 2hr

Table VIII. PC Component Attachment Study Test Matrix

Curing Temperature	Curing Time	Substrate thickness
120 °C	15 min.	0.5mm

EDA Sensor

In this section, the viability of the thermoforming process to achieve sensors for the measurement of electrodermal activity has been assessed. The sensors can be used to measure the sympathetic nervous system to classify the state of stress or anxiety. The tonic level, known as skin conductance level (SCL), slowly varies slightly on a time scale of tens of seconds. Rising and declining SCL is constantly changing within an individual respondent, depending on their hydration, skin dryness, or autonomic regulation. The phasic response rides on top of the tonic changes and shows significantly faster alterations. Variations in the phasic component are visible as "GSR bursts" or "GSR peaks". Phasic response is also labeled skin conductance response (SCR) as it is sensitive to specific emotionally arousing stimulus events (event-related SCRs, ER-SCRs). Fig. 5 depicts an additively fabricated thermoformed EDA sensing electrode alongside a mold part of a steering wheel. This includes conductive traces made of silver paste ink (Ag/AgCl) and a Polyethylene terephthalate glycol (PETG) substrate. Fig. 6 displays biosensors, including an Electrodermal Activity (EDA) sensor and a reference EDA sensor. The additively fabricated EDA sensor integrates a Microcontroller Unit (MCU) XIAO BLE nRF52840 Sense, amplifier, low-pass filter circuit, and voltage divider.

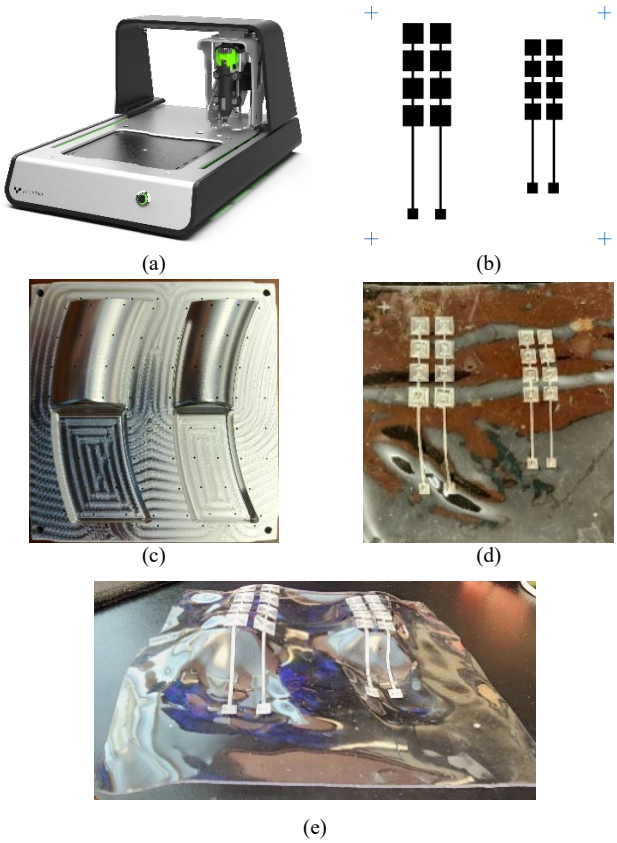

Fig. 5. (a) Voltera direct write printer with its (b) electrode design, (c) forming mold (d, e) formed sample

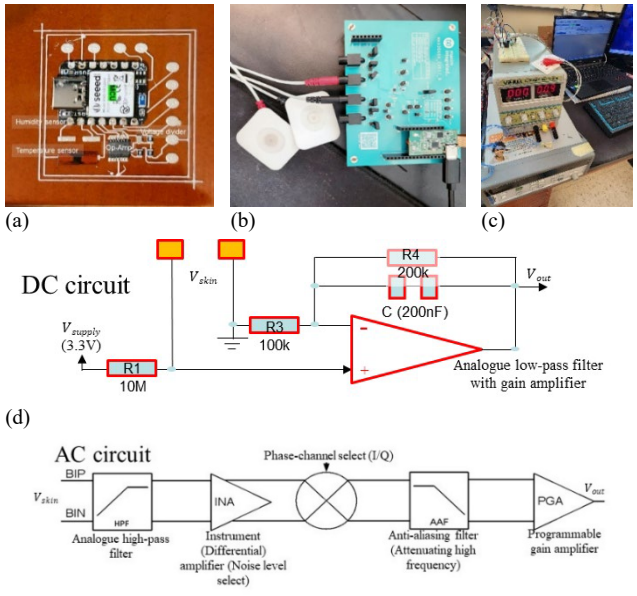

Fig. 6. (a) Fabricated biosensing board, (b) medical grade board MAX30009, (c) reference DAQ Agilent 34970A, (d) DC circuit, (e) AC circuit

Its biosignals are captured via serial communication with PuTTY, an open-source data acquisition software. The reference EDA sensor, a MAX30009 evaluation kit from Analog Devices Inc., uses built-in PC software for data acquisition. The MCU's firmware was programmed using CircuitPython, with Adafruit libraries for MCU operation, and coding was performed using the Mu-Python code editor. For the validation of accuracy of the setups, Agilent 34970A DAQ system was used, which has 10±0.007mA (0.07%) and 18bits (5.5 digits) of resolution.

RESULTS AND DISCUSSION

Direct Write

PXSXHX notation was utilized to categorize printed trace profiles under various print conditions. Here, P represents print pressure (in psi), S represents print speed (in mm/s), and H represents standoff height (in µm). For instance, P16S3H50 signifies a trace profile produced at a print pressure of 16 psi, a print speed of 3 mm/s, and a standoff height of 50 µm.

Print Process Study

In Fig. 7 following printing process parameters are constant: (i) Print Pressure is 14 psi; (ii) Standoff height is 70 µm (iii) The number of passes is one (iv) Temperature of sintering 70 (°C)/60 minutes.

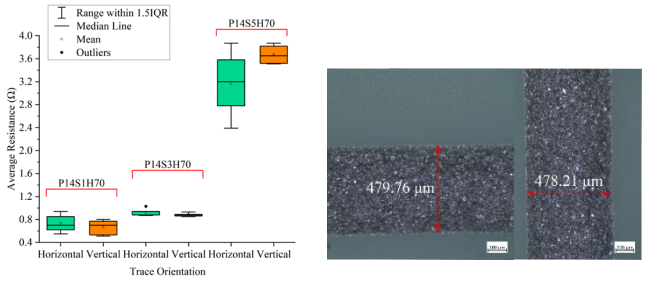

(a) (b)

Fig. 7. (a) Effect of print pressure and trace orientation on trace resistance for feature B, (b) optical images of traces

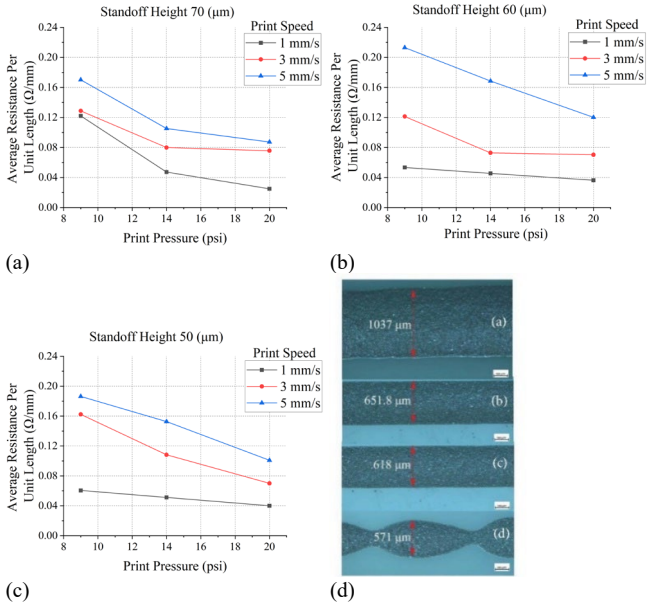

Fig. 8. Influence of print pressure and speeds on average trace R/L at (a) 70 µm, (b) 60 µm, (c) 50 µm print height, (d) Trace width from top to bottom: 1 mm/s, 3 mm/s, 5 mm/s, and 9 mm/s

Fig. 7 (a) illustrates the variation in resistance caused by changes in print direction and print speed. Five samples were employed for each direction to generate the box and whisker plot. While horizontal traces exhibit minimal differences compared to vertical traces, they generally agree well. Notably, the resistance variance in conductive traces is higher at lower and higher print speeds than at medium print speed. Fig. 7 (b) presents optical microscopic images of traces in different orientations under the same print condition. The observations reveal nearly equal widths of the traces. The measurement of white light interferometry is conducted using the Bruker Contour GT-K machine. In Fig. 8 (a), (b), and (c), the following printing process parameters are constant: (i) The number of passes is one (ii) the temperature of sintering 70°C/60 minutes. Fig. 8 (a), (b), and (c) depict how average trace resistance per unit length changes with print pressure for speeds of 1 mm/s, 3 mm/s, and 5 mm/s, maintaining constant print heights. Increased pressure decreases average R/L, while an upward trend is observed with higher print speeds. Fig. 8 (d) reveals trace width fluctuations with printing speed. Consistency diminishes as speed increases, with 9 mm/s showing inconsistent widths, defining an upper speed limit for reliable results.

Sintering Study

Fig. 9 illustrates the impact of sintering temperature and time on the resistivity of 3D-printed conductive traces, using the conductive trace profile P14S3H60 in this study. The test matrix for this investigation is presented in Table IV. The findings indicate a reduction in resistivity with an increase in sintering time, attributed to enhanced particle coalescence and greater particle-particle interaction during longer sintering periods, leading to improved conductivity. Additionally, a slight increase in resistivity is observed with temperature increments, potentially related to the heat deflection temperature (80°C) of the substrate material. This could lead to substrate deformation or softening as the sintering temperature approaches the heat deflection temperature of the substrate material.

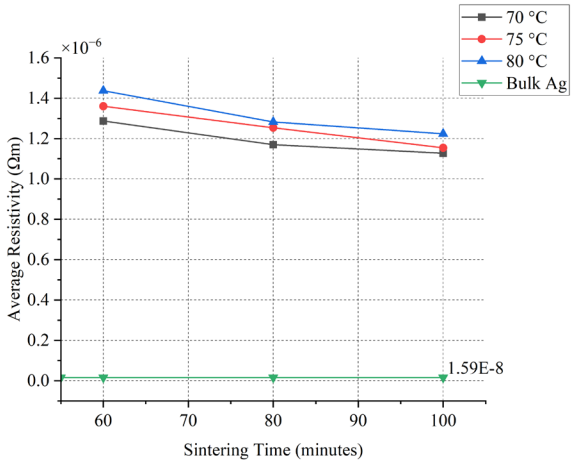

Fig. 9. Effect of sintering time and temperature on resistivity

Thermoforming Study with HIPS

This section presents the findings from the thermoforming study conducted on High Impact Polystyrene (HIPS) substrates on DIW platform, with a focus on how different thermoforming temperatures and times affect the resistance of conductive traces. All samples are printed with 7mm/s speed, 15psi pressure and 0.05mm standoff height based on the print process study. The study examined three distinct thermoforming temperatures (150°C, 175°C, and 200°C) and times (25s, 30s, and 35s). These conditions were specifically chosen to cater to the unique material properties of HIPS considering the heat deflection and Vicat softening temperature.

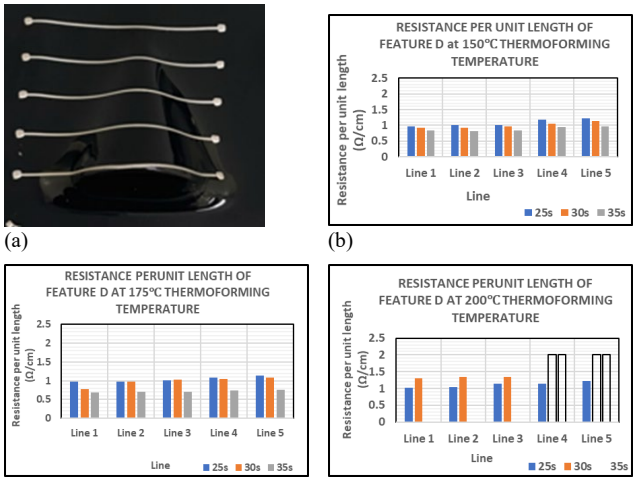

(a) (b) (c) (d)

Fig. 10. (a) Effect of thermoforming temperature and time on trace resistance for Feature A (a) aligned trace, (b) 150°C, (c) 175°C, (d) 200°C

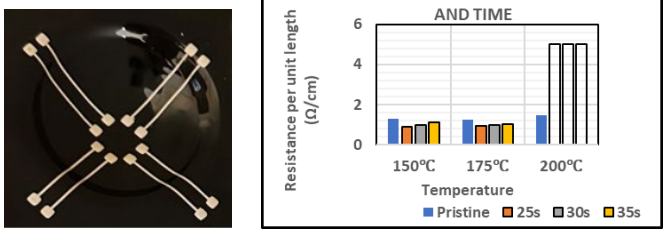

(a) (b)

Fig. 11. Effect of forming temperature and time on trace resistance for feature B (a) aligned trace, (b) R/L variation graph

Fig. 10 (a) shows the effect of thermoforming temperature and time on the traces of feature D. Fig. 10 (b) shows the resistance of feature D thermoformed at 150°C. The graph shows the resistance across each conductive line increased with the rise in the hump height, a trend consistent across all thermoforming times. A clear inverse relationship between resistance and thermoforming time emerged, as longer thermoforming time led to lower resistance. The same trend can be observed at thermoforming temperature of 175°C (see Fig. 10 (c)). However, at this intermediate temperature, each conductive line showed lower resistance and better conformity to the mold. This indicates improved performance compared to the 150°C. Fig. 10 (d) shows the result of thermoforming at 200°C, the sample exhibited signs of over-curing, leading to crack formation. These cracks significantly increased resistance and, in cases of prolonged

thermoforming time, resulted in the creation of open lines shown with un-filled bars in the graph. Fig. 11 (b) shows the resistance of feature A at varying temperature and time. It can be seen that resistance decreases after thermoforming for all the thermoforming time. This is basically because the sample undergoes further curing during thermoforming. At high thermoforming temperature (200°C), open lines are recorded which is due to over curing as seen in feature D. In general, the thermoforming study on HIPS substrates demonstrates that the resistance of conductive traces is significantly influenced by both the temperature and duration of the thermoforming process. Lower temperatures (150°C and 175°C) generally resulted in increased resistance with heightened hump height, but longer thermoforming times consistently reduced resistance, improving the conductive trace's performance. The intermediate temperature of 175°C was found to be optimal in balancing resistance reduction and mold conformity. Conversely, at 200°C, over-curing was a predominant issue, leading to increased resistance and the detrimental formation of open lines. These findings underscore the importance of precisely controlling thermoforming conditions to optimize the electrical properties and structural integrity of conductive traces on HIPS substrates.

Gravure Offset

Thermoforming study with 0.25 mm PC

For this thermoforming study with PC, ink A has been cured at a higher temperature than the recommended but for half the time so as to investigate the potential for process acceleration. Fig. 12 (a) depicts the resistance and the stretch ratio for the individual lines plotted against the distance from the center of the feature. The first three lines show the maintenance of the resistance ratio due to the feature topology, whereas the bottom four show a resistance ratio lesser than 1, i.e., the post-thermoforming resistance as compared to the pre-thermoforming resistance, which can be attributed to the additional sintering of the printed lines during the thermoforming process. The resistance and stretch ratios show a proportional trend as per the line location w.r.t. the center.

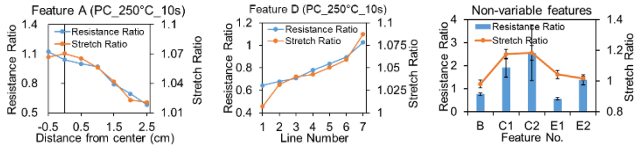

(a) (b) (c)

Fig. 12. (a) Resistance and stretch ratio variation across lines of feature A, (b) Results for feature D, (c) Results for non-variable features

Fig. 12 (b) demonstrates consistent findings for feature D: higher hump height correlates with inc reased resistance ratio and stretch ratio. Fig. 12 (c) presents averaged resistance and stretch ratios for non-variable features B, C1, C2, E1, and E2. C1 and C2 exhibit the highest ratios due to their elongation and sharp corners. Fig. 13 (a), (b), and (c) displays images of C1, C2, and thermoformed samples at 225°C for 15s, 20s, and 25s, illustrating that both time and temperature directly impact sample conformity to the mold. Fig. 14 displays how resistance and stretch ratios change with different forming temperatures and times. Increasing forming temperatures require shorter times for good mold conformity without substrate wrinkling. Hence, only three forming time durations have been tested for each forming temperature and the rest have been marked as DNT (did not test). However, higher temperatures lead to increased post-forming resistance due to ink over-curing, resulting in more no-connects. For PC substrate with ink 'A' traces, optimal forming involves lower temperatures for slightly longer durations to balance conformity and trace resistance. Table IX summarizes the impact of temperature-time combinations on formed substrate quality.

(a) (b) (c)

Fig. 13. Feature C images formed at 225°C for (a) 10s, (b) 15s, (c) 20s

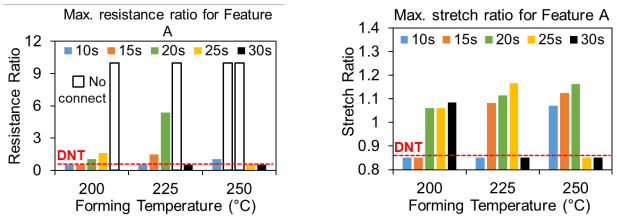

(a) (b)

Fig. 14. Forming variation with temperature and time for Feature A (a) Resistance ratio (b) Stretch ratio

Table IX. Results summary for PC substrate forming

Forming Time (s)	Forming Temperature (°C)		
	200	225	300
10	-	-	Low conformity
15	-	Low conformity	✓
20	Low conformity	✓	Wrinkling
25	✓	Wrinkling	-
30	Wrinkling	-	-

Thermoforming study with PETG

The study found that PC substrates can be thermoformed at different temperatures with adjusted times. Hence, for PETG, only one thermoforming temperature (125°C) was used with four times ranging from 25 to 34 seconds. Fig. 15 displays the resistance and stretch ratio results for both variable and non-variable mold features, mirroring trends observed in PC.

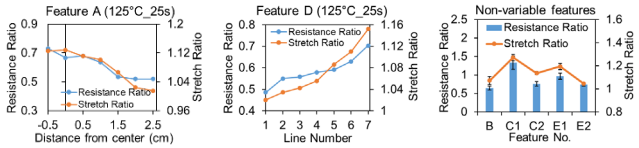

(a) (b) (c)

Fig. 15. (a) Feature A results, (b) Feature D results, (c) non-variable feature

The post-forming resistance for PETG traces is notably lower than for PC due to ink under-sintering at 70°C for 1 hr., much lower than the recommended ink sintering temperature. Consequently, the incomplete pre-forming sintering results in complete sintering during the 125°C forming process. Fig. 16

depicts the thermoformed sample at 30s. PETG substrate exhibits better thermoforming with less wrinkling and good conformity compared to PC. This difference arises from material properties and substrate thickness; PETG, being twice as thick as PC, is stiffer, resulting in cleaner thermoformed samples.

Fig. 16. Thermoformed PETG sample (34s at 125°C)

Component attachment study with PETG

In this section, component attachment on PETG has been studied. The component attachment study involves a two-step curing process: initial ink curing at 50°C for 30 min, followed by ECA curing at 70°C for 1hr or 2hr to prevent overcuring. Fig. 17 (a) shows a thermoformed sample with attached components, while Fig. 17 (b) illustrates pre- and post-thermoforming component resistance under different curing conditions. Pre-forming, the component resistance is higher due to partial ECA curing at 70°C, leading to more electrical no-connects. Thermoforming of PETG samples at 125°C for 31s, the optimal condition from thermoformability tests, further cures the ink and ECA, significantly reducing post-thermoforming resistance and electrical no-connects. The ECA curing time of 2hrs. leads to much better post-forming resistance relative to 1hr. ECA curing. Table X shows the process profile for PC substrate.

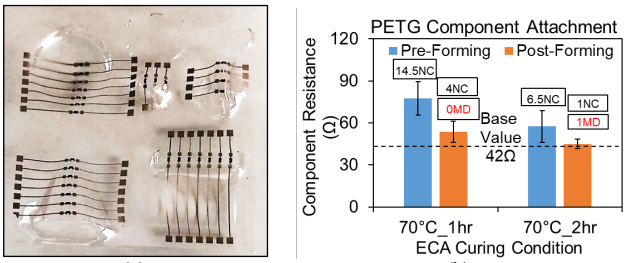

(a) (b)

Fig. 17. (a) Formed PETG sample with components attached, (b) Component attachment results

Table X. Component attachment profile for 0.5 mm PETG substrate

Ink curing	ECA curing	Forming
50°C for 30 min.	70°C for 1 hr.	125°C for 31 sec.

Component attachment study with PC

Since 0.25 mm thick PC showed wrinkling during the trace thermoforming study, a 0.5 mm thicker PC substrate was chosen for this study. Fig. 18 shows the image of the unwrinkled thermoformed sample and the pre- and post-forming component resistance results. Table XI shows the process profile for PC substrate.

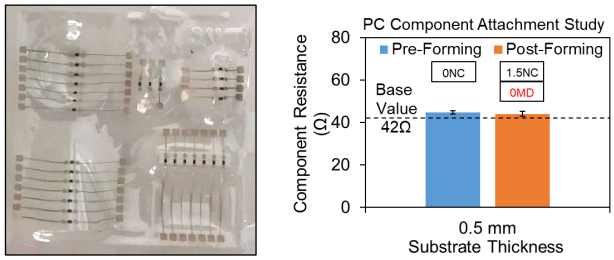

(a) (b)

Fig. 18. (a) 0.5 mm thick formed PC substrate, (b) Component attachment

Table XI. Component attachment profile for 0.5 mm PC substrate

Ink curing	ECA curing	Forming
100°C for 10 min.	120°C for 15 min.	200°C for 39 sec.

EDA Sensor

In this section, a series of functional tests were conducted on additively fabricated EDA boards-sensor pairs, and compared with medical grade EDA evaluation boards-sensor pairs in addition to cross-pairs to assess the accuracy of sensor alone or board alone. Additionally, a signal filter was designed to enhance bio-signal processing. The fabricated biosensor demonstrated a fixed gain of 3, in contrast to the medical grade evaluation board's variable gain, which ranged from 1 to 10. The fabricated board incorporates a 3.98Hz analog low-pass filter, while the reference board uses a variety of analog filters, details of which are discussed later in the paper. Fig. 19 illustrates the fast Fourier transform (FFT) analysis of the bio-signals from both our fabricated sensor (DC) and the reference sensor (AC). FFT is crucial in identifying the frequencies of both the bio-signal and noise. The analysis indicates that fabricated EDA sensor's signal displays bio-signal frequencies at 0.001Hz to 2Hz, with a predominant noise frequency around 10, 20, 30, 40 and 50 Hz. In these regards, both sensors generally used the same signal filter cut-off frequency, with a low-pass filter set at 3.98Hz and a high-pass filter at 0.004Hz, except during tests comparing different cut-off frequencies.

For comparison and validation of fabricated EDA measurement board as well as the Maxim board with thermoformed EDA sensing electrode, Agilent DAQ and 3M medical grade EDA sensing electrode were used. Fig. 19 depicts comparison of bio-signals between AC measurement (Maxim board) and DC measurement (Agilent) with medical grade EDA sensing electrode (3M) in multi-channels. The graph indicates that both EDA board display similar bio-signal characteristics, affirming their functional reliability. Fig. 20 shows simultaneous comparison of bio- signals between medical grade EDA sensing electrode (3M) and fabricated thermoformed electrode with Maxim board. The graph shows the fabricated sensing electrode behavior is identical to medical grade sensor. Fig. 21 portrays Comparison between Maxim board and fabricated board for the EDA measurement with medical grade EDA sensing electrode. The graph shows the fabricated EDA measurement board has similar characteristics and behavior as compared to medical grade EDA board.

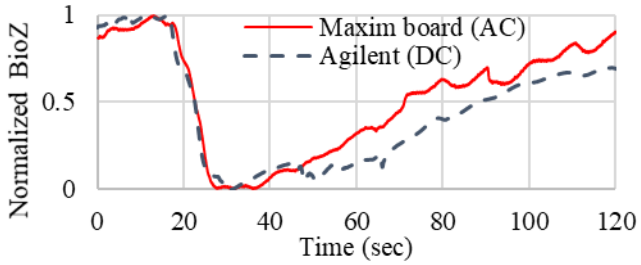

Fig. 19. Comparison of biosignals between AC Measurement (Maxim board) and DC Measurement (Agilent) with medical grade EDA sensing electrode (3M) in multi-channels

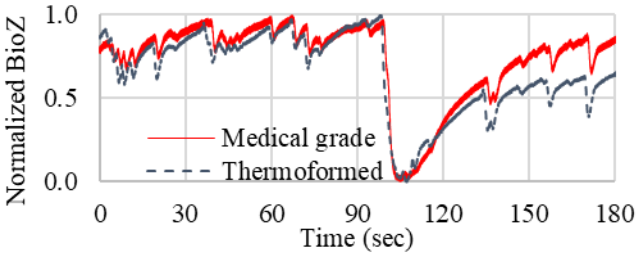

Fig. 20. Simultaneous comparison of biosignals between medical grade EDA sensing electrode (3M) and fabricated thermoformed electrode with Maxim board

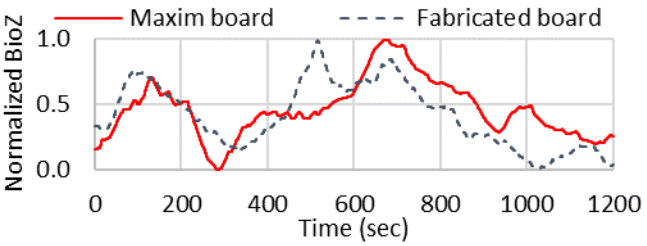

Fig. 21. Comparison between Maxim board and fabricated board for the EDA measurement with medical grade EDA sensing electrode

SUMMARY AND CONCLUSIONS

The study explored printed electronics' suitability for in-mold electronic circuits. The study explored the effects of print parameter variations of direct ink write systems on the final thermoformed traces on PETG, PC, and HIPS samples. Gravure offset printing made conductive traces on PC and PETG substrates. PC had a narrow thermoforming range, needing precise temperature and time for acceptable results. PETG, more formable due to material and thickness, showed lower post-thermoforming resistance than PC, affected by under-sintering owing to PETG's low heat deflection temperature. A component attachment study using ECA on PETG shaped the ink and ECA curing profile for thermoformed full wave rectifier demonstrator circuits. DIW based thermoformed biosensor with PETG substrate was able to measure precisely EDA signal.

ACKNOWLEDGMENTS

The project was sponsored by the NextFlex Manufacturing Institute under PC7.6 Project titled - In-Mold Electronics Interconnection and Thermoforming for 3D-Integrated Applications. This material is based, in part, on research sponsored by Air Force Research Laboratory under agreement number FA8650-20-2-5506, as conducted through the flexible hybrid electronics manufacturing innovation institute, NextFlex. The U.S. Government is authorized to reproduce and distribute reprints for Governmental purposes notwithstanding any copyright notation thereon. The views and conclusions contained herein are those of the authors and should not be interpreted as necessarily representing the official policies or endorsements, either expressed or implied, of Air Force Research Laboratory or the U.S. Government.

REFERENCES

[1] J. Trommnau, J. Kühnle, J. Siegert, R. Inderka and T. Bauernhansl, "Overview of the state of the art in the production process of automotive wire harnesses current research and future trends", Procedia CIRP, vol. 81, pp. 387-392, 2019.

[2] Reif K. Bosch, "Autoelektrik und Autoelektronik: Bordnetze Sensoren und elektronische Systeme; mit 43 Tab. 6th edn", Wiesbaden: Vieweg+Teubner Verlag / Springer Fachmedien Wiesbaden GmbH Wiesbaden, 2011.

[3] Ernst M and M. Heuermann, "Die wichtigsten Bordnetz-Trends", Elektronik automotive, pp. 20-23, 2014.

[4] A2MAC1 EURL. A2MAC1 Automotive Benchmarking, December 2018, [online] Available: https://portal.a2mac1.com/.

[5] Y. Yamano, T. Hosokawa, H. Hirai, J. Ono, T. Otsuka, M. Tabata, et al., "Development of aluminum wiring harness", SEI technical review, vol. 73, pp. 73-80, 2011.

[6] R. Rius and Armand, A novel optimization methodology of modular wiring harnesses in modern vehicles: weight reduction and safe operation, 2017.

[7] T. Alajoki, M. Koponen, A. Huttunen, M. Tuomikoski, et al., "Hybrid in-mould integration", 46th International Symposium on Microelectronics IMAPS, 2013, 188 – 193.

[8] Newswire, IDTechEx research analyzes in-mold electronics, https://www.newswire.com/news/idtechex-research-analyzes-in-mold-electronics-starting-simple-to-21098388, February 2020.

[9] ASTM D648-18, Standard test method for deflection temperature of plastics under flexural load in the edgewise position, April 2018.

[10] ASTM D1525-17e1, "Standard Test Method for Vicat Softening Temperature of Plastics", https://www.astm.org/d1525-17e01.html, September 2017, accessed: May 2023.

[11] K. Srinivas, "Heat deflection temperature (HDT) and Vicat softening temperature testing", https://advanses.com/heat-deflection-temperature-vicat-softening-temperature, February 2022, accessed: May 2023.

[12] J. Wiklund, A. Karakoç, T. Palko, H. Yigitler, et al., "A Review on Printed Electronics: Fabrication Methods, Inks, Substrates, Applications and Environmental Impacts." Journal of Manufacturing and Materials Processing, 2021.

[13] M. Beltrão, F. Duarte, J. Viana, V. de Paulo, "A review on in-mold electronics technology", Polymer Engineering & Science, 2022.